Selection of Artificial Muscle Actuators for a Continuum Manipulator

Devin R. Berg [1,2,*], **Perry Y. Li** [2] **and Arthur G. Erdman** [2]

[1] *Engineering and Technology Department, University of Wisconsin-Stout, Menomonie , Wisconsin, USA*
[2] *Department of Mechanical Engineering, University of Minnesota, Minneapolis, Minnesota, USA*

Correspondence*:
807 3rd St. E., Menomonie, WI 54751, USA
bergdev@uwstout.edu

ABSTRACT

Artificial muscle actuators have become a popular choice as actuation units for robotic applications, particularly in the growing area of soft robotics. The precise specification of an artificial muscle actuator for a particular application requires the consideration of several parameters that work together to achieve the performance characteristics of the actuator. This paper explores the specification of artificial muscle actuator parameters by presenting and applying the analytical description of the actuator, simulation by finite element method for investigating material stresses under a wide variety of configurations, and a specific parameter selection process. This is followed by an experimental validation using an example actuator to compare against the predicted actuator performance. Some discussion of appropriateness of this type of actuator as a candidate solution for use in the example application of a dexterous continuum manipulator is included.

Keywords: actuation, artificial muscle actuators, hydraulics, medical robotics

1 INTRODUCTION

Considering the selection of actuators to power a robotic manipulator is a particularly important aspect of robotic design. Some of the possibilities include electromechanical linear actuators, pneumatic actuators, or hydraulic actuators. A comparison of these three choices reveals that each option has both advantages and disadvantages. Electromechanical actuators are typically considered to be more efficient than their pneumatic and hydraulic counterparts, while hydraulic actuators have the highest power to weight ratio of the three choices presented here, assuming that the hydraulic power source is located remotely Granosik and Borenstein (2006). As a means of providing example design constraints, a continuum manipulator designed for minimally invasive natural orifice surgery was selected as a platform for investigation. The device in question is described in full in Berg, 2013 Berg (2013c). Providing consideration for the stringent requirements placed on such a manipulator for natural orifice surgery, it was determined that the size restriction due to the nature of natural orifice surgery was the most critical condition to be met, followed by the force output from the device that is necessary to achieve desired performance, approximately five newtons Berg et al. (2011). Therefore, hydraulic actuation was chosen for its higher power output despite any possible lack in efficiency, which is less critical in surgical applications.

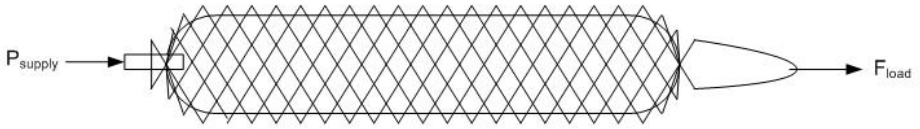

Figure 1. Artificial muscle actuator.

Although hydraulic actuation offers high power density, mechanical rigidity and high dynamic response, the force capability, F, for a given pressure, P, of a conventional linear hydraulic actuator is limited by the piston area, A, given by: $F = P \cdot A$. In view of the stringent diametric requirement of the present application, the use of hydraulic artificial muscle actuators (AMA) (see Fig. 1), which will be shown to have better peak force capability than conventional linear actuators for the same pressure and diameter, is of interest Schulte (1961). While the concept of artificial muscle actuators and their use in robotics is not new, the majority of application use pneumatic power to drive them Cardona (2012); Trivedi et al. (2008a); Klute and Hannaford (2000); Tsagarakis and Caldwell (2000). However, through the use of a hydraulic medium it may be possible to mitigate some of the issues with responsiveness and rigidity that have been encountered previously. There are two important advantages to a hydraulic approach: 1) a higher pressure (by a factor of 10 compared with pneumatic) can be applied so that force and power density can be further increased and the actuator diameter can be decreased; 2) liquid has a much lower compressibility and therefore better rigidity than compressed gas.

Artificial muscle actuators consist of a contained internal bladder, surrounded by a flexible, braided outer sheath. It is the geometry of this outer sheath that transmits the radial expansion of the internal bladder due to applied pressure to contractile force along the longitudinal axis of the muscle actuator Davis et al. (2003). As the radius of the bladder, and thus the outer mesh, increases, the individual strands of the mesh which are woven in a over-under crossing pattern rotate relative to each other and to the long axis of the actuator and shorten the longitudinal distance from one end of the strand to the other. The load capacity of the artificial muscle actuator is then a function of the geometry and orientation of the outer sheath and the pressure applied to the internal bladder Chou and Hannaford (1996).

2 ANALYTICAL DESCRIPTION OF ARTIFICIAL MUSCLE ACTUATORS

There are two methods presented in the literature for modeling the transmission of internal pressure to contractile force of an AMA. The first is a theoretical approach based upon energy conservation Schulte (1961), while the second is an examination of the force profile of the surface pressure Tondu et al. (1996). The first approach is based on the principle that energy supplied to the actuator by the pressurized fluid must leave the actuator through the application of a load over some distance. The second approach is based on an examination of the distortion of the internal bladder under isobaric conditions. However, ultimately each of these methods arrives at the base model Tsagarakis and Caldwell (2000). A summary of the first method is presented here. It should be noted that this model does not account for possible effects of compressibility in the bladder, interactions between the bladder and the braided outer sheath, or any contribution from the ends of the muscle actuator.

As shown in Fig. 2, adapted from Chou and Hannaford Chou and Hannaford (1996), it is first necessary to define the geometric parameters of the braided sheath. These parameters include the length of the individual braided strands, b, the number of turns each strand makes over the length of the actuator, n, and the angle

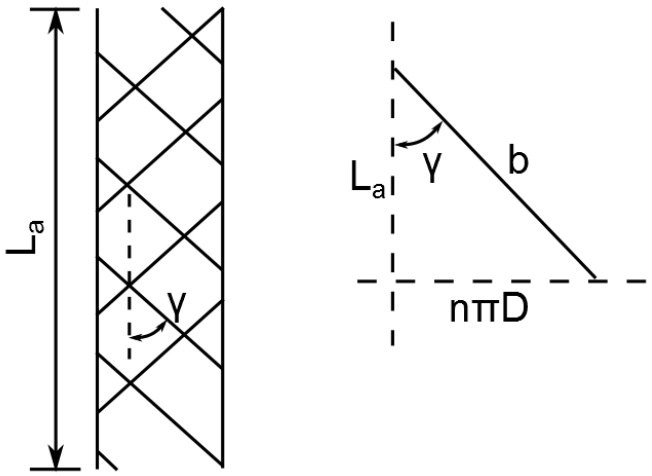

Figure 2. Artificial muscle actuator geometry (left) and magnified view of braid geometry relationship for a single unwound strand (right).

between the strands and the longitudinal axis of the actuator, $\gamma(t)$, which is assumed to be uniform for all strands within the braided sheath.

The overall length of the actuator, $L_a(t)$, and the actuator diameter, $D(t)$, can then be represented in terms of the constants, n and b, and as functions of the variable $\gamma(t)$, as seen in Eq. (1) and Eq. (2).

$$L_a(t) = b \cdot \cos\gamma(t) \tag{1}$$

$$D(t) = \frac{b \cdot \sin\gamma(t)}{n\pi} \tag{2}$$

Then, calculating the volume of a cylinder and substituting in the functions for $L_a(t)$ and $D(t)$,

$$V(t) = \frac{\pi}{4} D(t)^2 L_a(t) = \frac{b^3}{4\pi n^2} \cdot \sin^2\gamma(t)\cos\gamma(t). \tag{3}$$

The first derivatives of $L_a(t)$ and $V(t)$ with respect to $\gamma(t)$ are calculated as

$$\frac{dL_a(t)}{d\gamma(t)} = -b \cdot \sin\gamma(t) \tag{4}$$

$$\frac{dV(t)}{d\gamma(t)} = \frac{b^3 \sin\gamma(t)}{2\pi n^2} \cdot (\cos^2\gamma(t) - \frac{1}{2}\sin^2\gamma(t)) \tag{5}$$

From Eq. (4) and Eq. (5), the first derivative of $V(t)$ with respect to $L_a(t)$ is given as

$$\frac{dV(t)}{dL_a(t)} = \frac{dV(t)/d\gamma(t)}{dL_a(t)/d\gamma(t)} = \frac{-b^2}{4\pi n^2} \cdot (3\cos^2\gamma(t) - 1). \tag{6}$$

From the principle of virtual work we have:

$$F_a(t) \cdot dL_a(t) = P_a(t) \cdot dV(t) \tag{7}$$

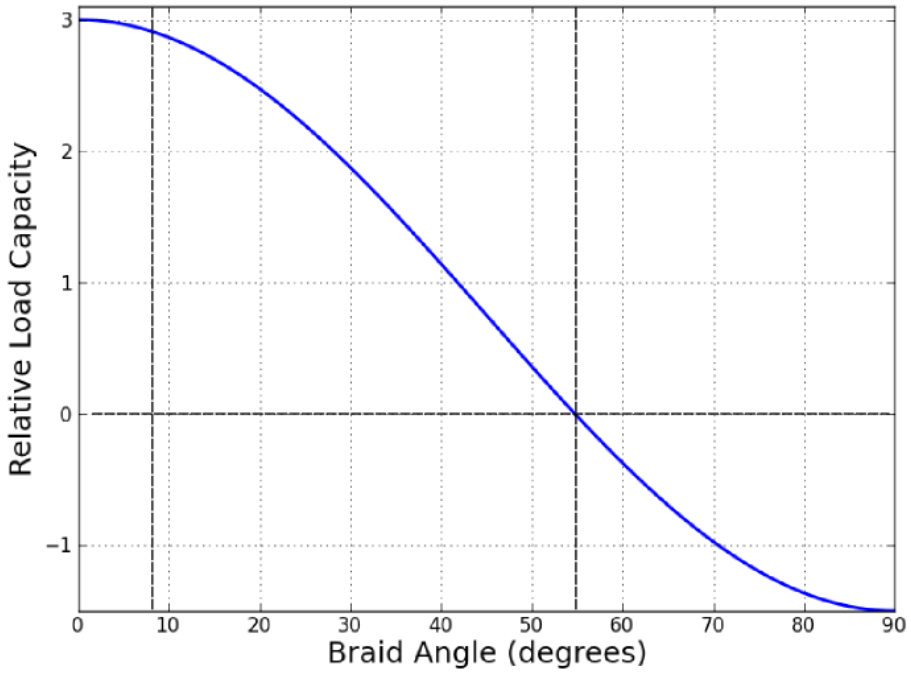

Figure 3. Ratio of force capacity for artificial muscle actuator to force capacity of a piston and cylinder when the maximum cross-sectional area of each actuator is equivalent ($F = P \cdot A_{max}$) as a function of braid angle.

and solving Eq. (7) for the force output with Eq. (1 and 6) results in

$$F_a(t) = P_a(t)\frac{b^2}{4\pi n^2} \cdot \left[3\frac{L_a(t)^2}{b^2} - 1\right] \tag{8}$$

$$= P_a(t)\frac{b^2}{4\pi n^2} \cdot \left[3\cos^2(\gamma(t)) - 1\right] \tag{9}$$

$$= P_a(t)\frac{\pi D(t)^2}{4} \cdot \left[\frac{3\cos^2(\gamma(t)) - 1}{\sin^2(\gamma(t))}\right] \tag{10}$$

where $F_a(t)$ is the contractile force and $P_a(t)$ is the pressure differential across the bladder wall. Because the term within the brackets in Eq. (9) can be greater than 1 ($\lim_{\gamma(t)\to 0} = 2$), the force capability of a artificial muscle can be greater than that of a hydraulic piston actuator for the same area and pressure. It is assumed here that the force from the hydraulic piston actuator is $F = P \cdot A$ where the diameter is equivalent to the maximum diameter of the AMA. In reality the available area may be reduced by the piston rod cross-sectional area. Notice, however, that this advantage comes at the cost of having the force/pressure relationship vary with $\gamma(t)$ or actuator length $L_a(t)$, illustrated in Fig. 3. When the contraction angle is $35.3°$, the two actuators are equivalent. Further, it can be seen (Fig. 3) that the maximum braid angle (full muscle contraction) occurs when $\gamma = 54.7°$. This result can be demonstrated by looking at Eq. 9 and setting the contraction force, F_a, equal to zero then solving for the braid angle, γ. Thus this maximum value for γ is thus independent of all other parameters and holds true under all conditions.

Refinements to this basic model have been presented in the literature which include considerations for bladder end cap geometry, non-linear bladder material response, and frictional effects Klute and Hannaford (2000); Tsagarakis and Caldwell (2000); Chou and Hannaford (1996). However, the basic model has been

experimentally shown to provide sufficient accuracy to gain an understanding of the theoretical system performance without introducing unnecessary model complexity Davis and Caldwell (2006).

3 BRAID PARAMETER SELECTION

When designing an artificial muscle actuator for a given application, it is likely that the available supply pressure is known as well as the desired length, L_{max}, and maximum diameter, D_{max}, of the actuator which occurs when the braid angle, $\gamma = 54.7°$. Therefore, the optimal design is the one that maximizes the performance of the actuator in terms of the range of the muscle contraction. Due to the geometric constraints of the AMA as discussed in Section 2, the contraction range is directly tied to another important geometric property, the range of possible braid angles throughout the stroke of the AMA. The minimum braid angle (full muscle extension) is dependent on the strand diameter, D_s, and the number of strands in the braid, N, and occurs when adjacent strands make contact Davis and Caldwell (2006). This relationship is presented as

$$\gamma_{min} = \frac{1}{2}\sin^{-1}\left(\frac{D_s N}{\pi D_o}\right) = \frac{1}{2}\sin^{-1}\left(\frac{D_s N^2}{b}\right) \tag{11}$$

where $D_o = \frac{b}{\pi n}$ (obtained by evaluating Eq. 2 at $\gamma = 90°$)is the theoretical maximum muscle diameter. Recalling Fig. 3 which shows a plot of the relative force capacity of the artificial muscle actuator versus the braid angle of the mesh, it is possible to see that the force goes to zero when the braid angle reaches $54.7°$ as previously mentioned. The upper limit of the force, which is dictated by the minimum achievable braid angle, is shown by the left vertical line. This line can shift left or right based upon the characteristics of the mesh, D_s and N.

Therefore, it is necessary to consider the possible combinations of strand diameter, D_s, and number, N, in order to optimally design the AMA. This can be done by minimizing the braid angle, γ_{min}. Additionally, the stress within each individual strand of the braided mesh must also not exceed the limits of the mesh material and thus acts as a constraint on the determination of γ_{min}. The tensile stress within an individual strand within the braid is presented in the literature Davis and Caldwell (2006) as

$$\sigma(t) = \frac{P_a(t)D(t)L(t)}{2nNA_{strand}} = \frac{2PD_o^2\sin^2\gamma(t)\cos\gamma(t)}{ND_s^2} \tag{12}$$

which is formulated by analyzing the fractional component of the hoop stress realized within an individual strand of the braided mesh. Each of the N strands encircles the bladder n times. This result can then be compared against the tensile limit of the mesh material, which is typically either a nylon polymer ($\sigma_Y \approx 50MPa$) or stainless steel ($\sigma_Y \approx 500MPa$).

3.1 Finite Element Analysis of Internal Bladder

The use of the artificial muscle actuator as a means of power input to the system carries with it several advantages previously discussed. However, it is also necessary to understand the failure limits for each component. An expression for determining stress in the braided mesh was discussed in the previous section; however, it is necessary to understand the failure limits of the internal bladder due to applied pressure as well as the bladder is likely to be the weaker of the two components that make up the actuator. The likely mode of failure for the bladder is by the wall expanding through the gaps between strands, as shown in Fig. 4, of the braided mesh and rupturing Davis and Caldwell (2006). Further, it is desirable to avoid exceeding the elastic limit of the bladder material, which varies based on material composition and strain

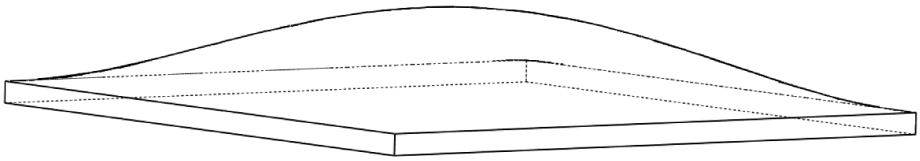

Figure 4. Illustration of the bladder mesh bulging through a gap in the strands of the braided sheath.

rate, estimated as 3 MPa for general latex rubber Hagan et al. (2009). Towards this end, a finite element analysis of stress within the bladder was performed for a variety of possible combinations of actuator design parameters. The relevant parameters of each diamond shaped unit segment of the bladder are then the edge length, EL, and the braid angle, γ, as shown in Fig. 5. The edge length is a constant measure of the mesh density and is determined in the manufacturing by setting the distance between subsequent strands. The value for the edge length can be calculated as

$$EL = \frac{b}{nN} = \frac{\pi D_0}{N} \tag{13}$$

where b, n, and N are the strand length, number of turns per strand, and strand number, respectively, as before. The braid angle is a measure of AMA contraction and thus changes as the AMA is pressurized. This relationship is described in Section 2. In addition to the parameters EL and γ, it is also necessary to consider the wall thickness, t, of the bladder material when determining a proper design to prevent failure. Further, the pressure within the bladder, P_a is an important consideration for evaluating the stress within the bladder wall. All of these possible variations make determination of the failure criteria for the internal bladder of the artificial muscle a difficult problem to evaluate. The complexity of this problem is further increased due to the intricacies of shell mechanics for an irregular shape. To simplify the analysis, the bladder was first divided into the smallest repeated unit which takes the form of a diamond where the sides are defined by the strands of the braided mesh, as shown in Fig. 5. The model used here assumes that the edges of the bladder segment are fixed in place by the braid strands. This assumption is reasonable as each side of a given segment is shared by adjacent segments which are each subject to the same conditions. Further, this model does not account for any stress relief that may be present due to the diameter of the strands restraining the bladder. This results in the overestimation of the stress within the bladder and thus means that the selection of parameters based on this model will be conservative.

A model of this individual unit was developed in the finite element analysis software package, Abaqus Unified FEA (Dassault Systèmes). As it is possible that each of these four parameters will vary independently, it is necessary to evaluate all possible combinations. To accomplish this, the input file was scripted using the Python programming language to allow for automation of the job submission process Berg (2013a). Briefly, the script was set up to evaluate for six possible edge lengths ($\in$ [0.25 mm, 1.5 mm]), six braid angles ($\in$ [5°, 55°]), five bladder thicknesses ($\in$ [0.05 mm, 0.25 mm]), and five internal pressures ($\in$ [0.25 MPa, 1.5 MPa]). This results in a total of 900 possible combinations of EL, γ, t, and P_a. The range for each parameter was selected to cover the likely range encountered by the AMA when used for this application. For each combination, the script defines the geometry of the bladder segment, applies the boundary conditions and pressure load, and submits the job to the solver.

An example of the results output by the Abaqus simulation is shown in Figs. 6 and 7 where the input parameters were set to [EL,γ,t,P_a]=[1.0 mm, 15°, 0.15 mm, 700 kPa]. Figure 6 shows the deformation

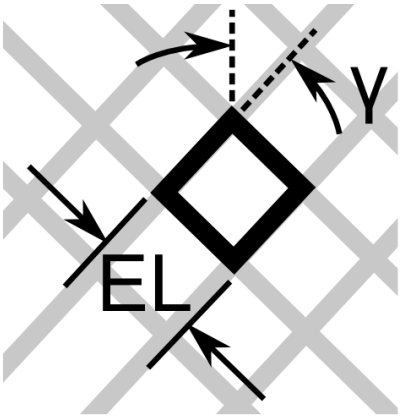

Figure 5. Graphic showing relevant planar dimensions describing an individual bladder segment.

of a bladder segment for a given set of parameters. As expected, the greatest deformation occurs at the center of the segment while the deformation at the edges is zero as specified by the boundary conditions. Here it is shown that the maximum calculated deformation is on the order of 0.5 mm for this example. Figure 7 shows the magnitude of the Von Mises stress within the bladder segment for the example set of parameters. Here it is shown that the highest stress concentration is calculated at the edge of the segment near the obtuse angle. The maximum stress at this location is on the order of 2.8 MPa. Moving away from the boundary, the next highest stress occurs at the same location as the maximum deformation within the segment (geometric center) and is on the order of 2.0 MPa.

The results from each of the 900 simulations (each combination of EL, γ, t, and P_a) were then stored in individual output files. The result of interest in this case is the maximum stress that occurs in the bladder segment. To extract this information from each of the results files, a post processing script was also written in Python to read the Von Mises stress data for each element in the mesh and then find the maximum Berg (2013a). This maximum Von Mises stress was then written to a text file along with the corresponding parameter values for each of the 900 simulations Berg (2013b). This text file represents a four dimensional array that can be used as a lookup table to find the stress corresponding to a given set of input parameters.

The array contains the values for maximum stress calculated under the given range of selected input parameters which thus necessitates the use of an interpolation to extract the relevant information for any one specific set of input conditions. For this, a cubic 4-dimensional interpolation function was used. As shown in Fig. 8, it was found that for any arbitrary set of input parameters where only the braid angle was varied the maximum stress occurred when the braid angle was 45° for all combinations of the inputs, P_a, N, and t. Note that the strand number, N, was used in place of EL for presentation of these results as it is more relevant as a design parameter. For a given value of N, EL is calculated using Eq. 13 for submission to the interpolation function. The value for D_0 was set to 6 mm for this application. This result for the braid angle is true for any set of input parameters and is not unexpected since the surface area of the diamond shaped unit of the internal bladder is largest when the braid angle is 45°. Based on this result, it would be appropriate to use a braid angle of 45° in subsequent calculations in order to account for the worst case scenario.

As discussed in Section 3, the strand diameter, D_s, and number, N, are the two critical parameters for design of the braided mesh. In terms of evaluating the bladder stress, strand diameter effects only the stress concentration at the boundaries of each bladder segment (larger strand diameter equates to lower stress concentration at the boundary). Thus assuming the most conservative condition, strand diameter is not

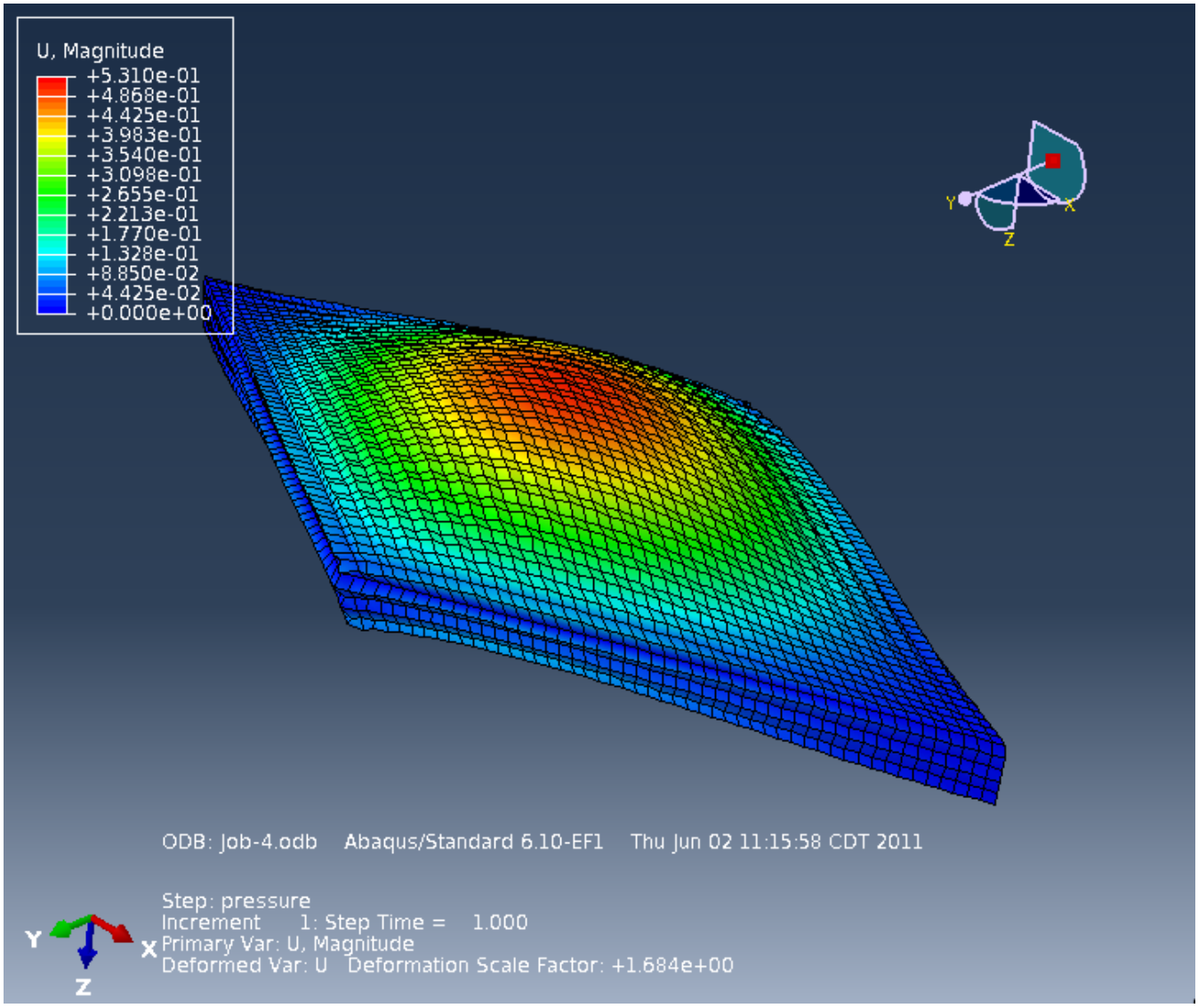

Figure 6. Example output of Abaqus simulation results for deformation of an internal bladder section.

factored into the calculation of the bladder stress. Instead, strand diameter is relevant in determination of failure within the braided mesh itself. An evaluation of the bladder stress was performed with respect to the effects of the various independent parameters. The braid angle was fixed at 45° while the strand number, N, actuator pressure, P_a, and bladder thickness, t, where varied individually. This analysis is shown in Figs. 9 - 11. First, it is shown in Fig. 9 that there is a direct linear relationship between actuator pressure and stress in the bladder wall. Thus a change in actuator pressure yields a proportional change in bladder stress with a constant of proportionality that ranged from 0.65 (N=80, t=0.25 mm) to 31.5 (N=16, t=0.1 mm).

Next, to look at the effects of strand number and bladder thickness, the actuator pressure was set to 700 kPa while the strand number, N, and the bladder thickness, t, were varied. As shown in Fig. 10 varying the strand number, N, shows that the bladder stress increases quickly as the strand number approaches 15 where the spacing between strands becomes large. Thus, for this application, the bladder stress can be used to set the lower limit for the strand number. It is desirable to approach this lower limit as fewer strands means that the performance of the actuator is better due to having a longer contraction range.

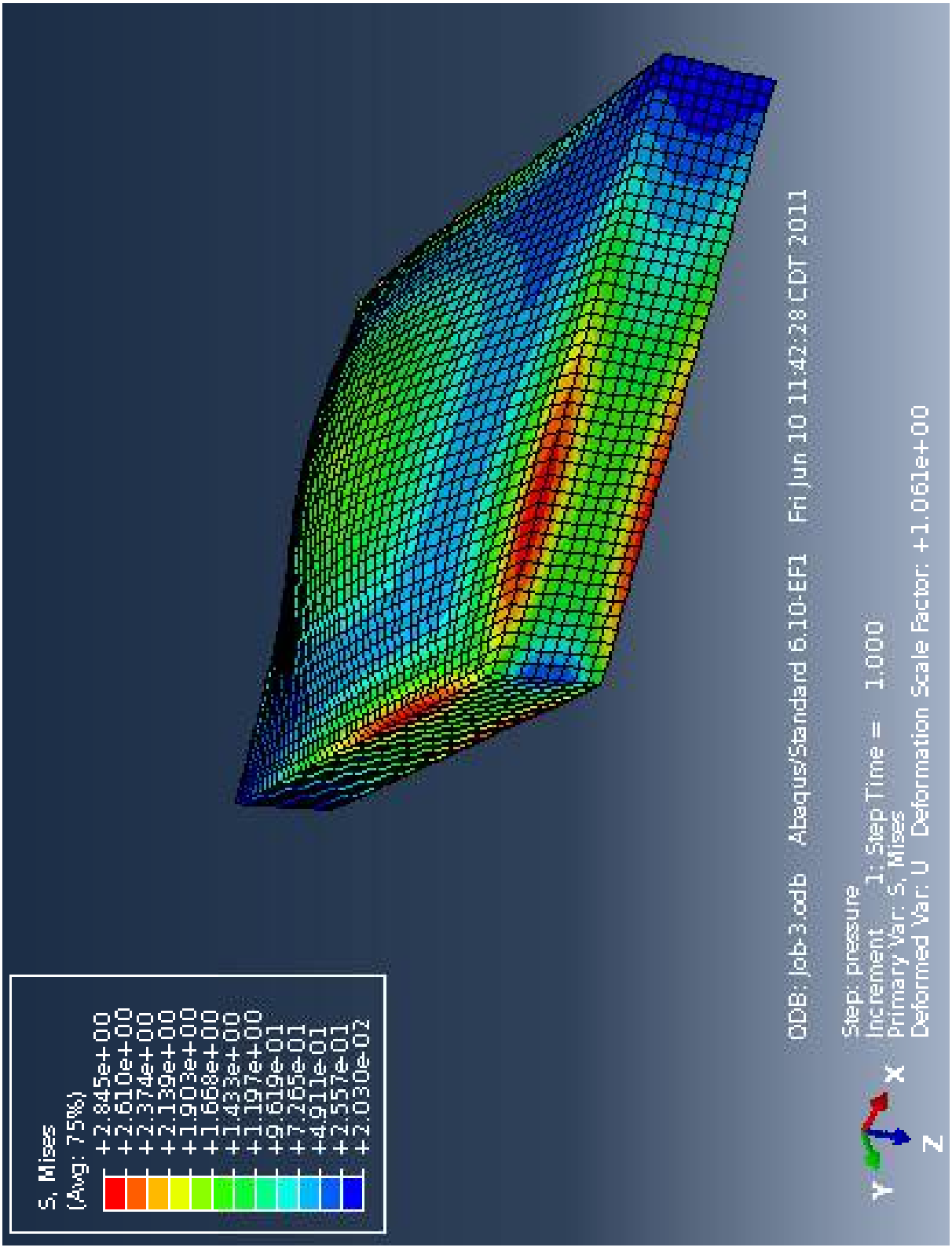

Figure 7. Example output of Abaqus simulation results for Von Mises stress of an internal bladder section.

Finally, the effect of bladder wall thickness were examined. Figure 11 shows that the wall stress increases quickly when the wall thickness is smaller than approximately 0.15 mm and changes more gradually above

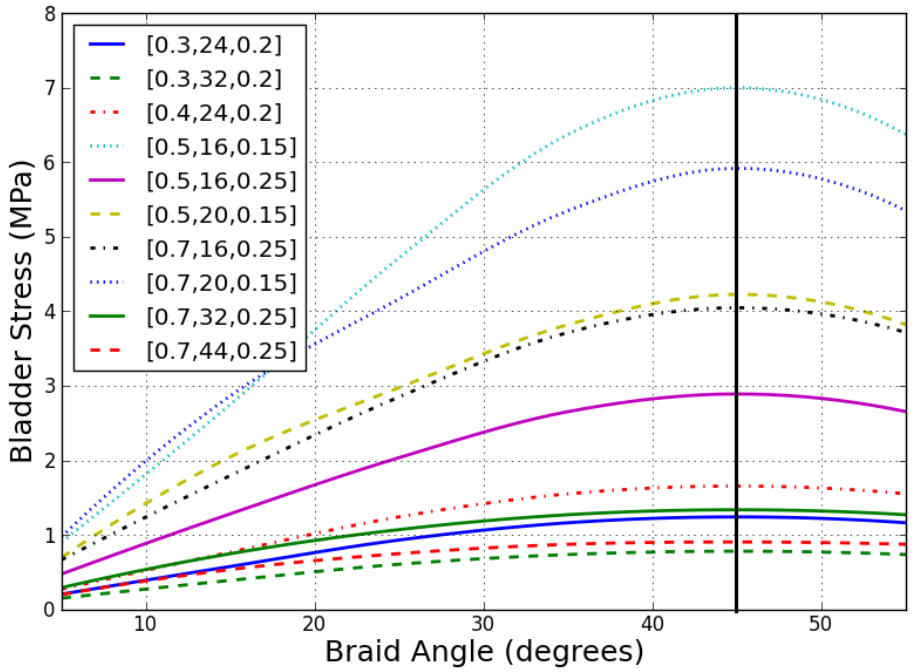

Figure 8. Calculation of maximum bladder stress for variable braid angle. Values indicated in the legend correspond to [P_a (MPa), N, t (mm)].

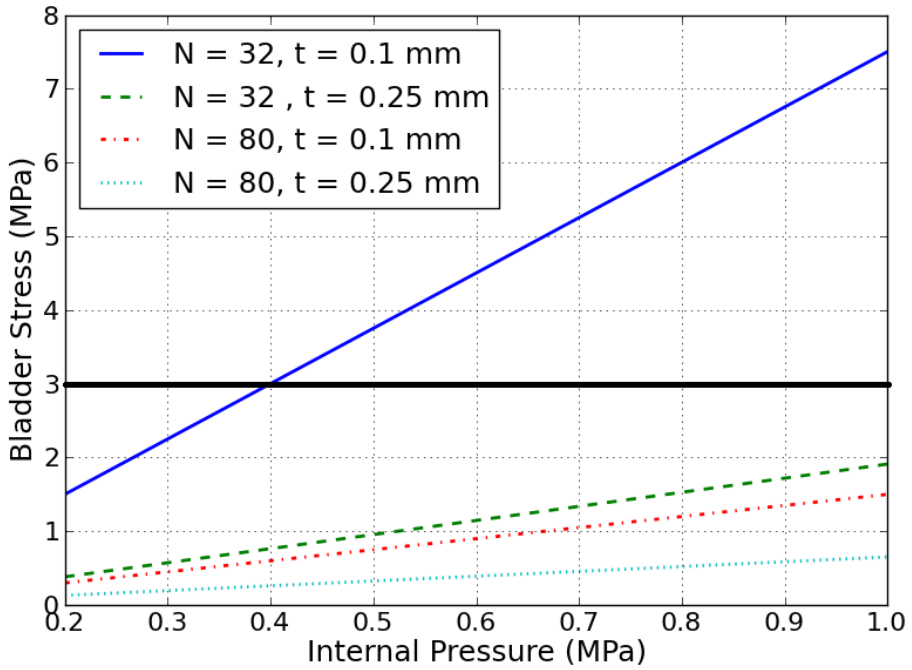

Figure 9. Plot of the bladder stress calculated using FEA versus actuator pressure. Braid angle is set to 45° for all cases.

that value. This result is important to consider as the bladder wall thickness plays a role in determining the minimum achievable diameter of the AMA.

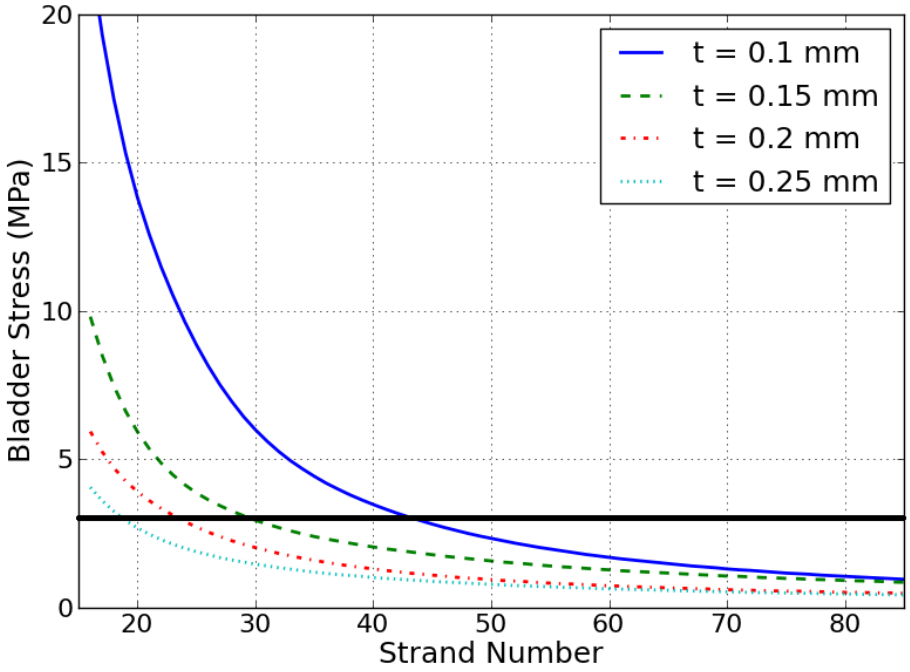

Figure 10. Plot of the bladder stress calculated using FEA versus strand number. Braid angle is set to 45° for all cases.

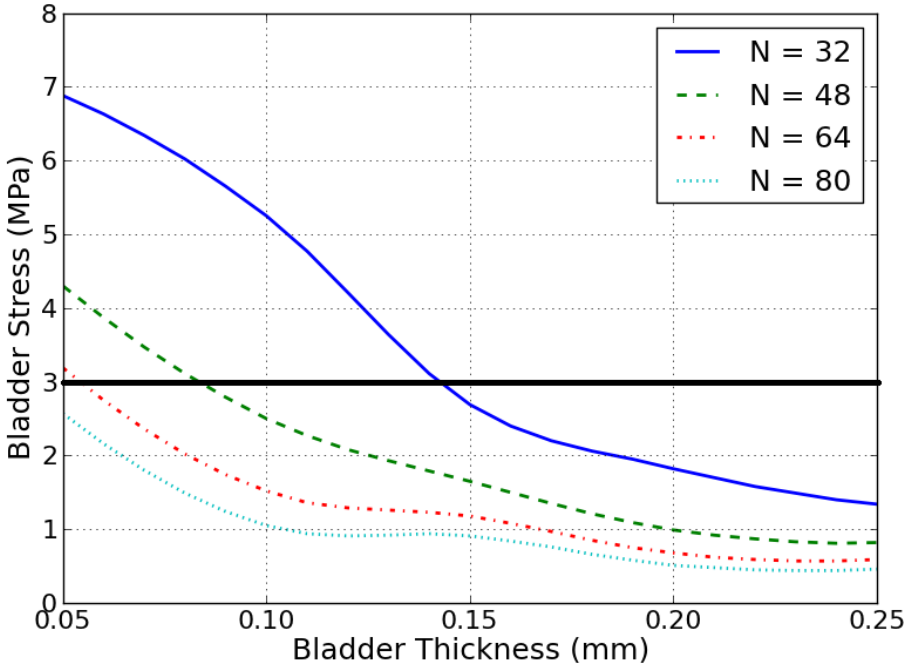

Figure 11. Plot of the bladder stress calculated using FEA versus bladder wall thickness. Braid angle is set to 45° for all cases.

3.2 Parameter Selection Methodology and Fabrication

The previous text provided a means of designing the AMA by analyzing the constraints in terms of strand stress and bladder stress for a given set of input conditions. Equation 12, when combined with the results

presented in Section 3.1, allows for a determination of the optimal combination of strand diameter, D_s, and strand number, N, within the braid for which the strand stress does not exceed the tensile strength of the braid material and the stress in the bladder wall does not exceed the limits of the bladder material. The thickness of the bladder wall is also an independent design parameter that can be minimized in order to allow the actuator to reach full elongation and therefore the wall thickness can be included as a design variable.

The strand diameter and number can then be used in the manufacture of an appropriate braided mesh. For the braiding machines that manufacture this sort of braided mesh, the necessary input parameter is the pick count or the number of times the strands cross the center line per unit length Omeroglu (2006). This input setting can be calculated from the optimized strand number, N, as

$$Pick = \frac{nN}{2L_c} \tag{14}$$

where the length, L_c, is the actuator length at the diameter of the core, D_c (independent parameter as long as it is smaller than D_o), that the mesh is being braided onto such that Eqs. 1 and 2 become

$$L_c = b \cdot \cos\gamma_c \tag{15}$$

$$\gamma_c = \sin^{-1}\left(\frac{\pi n D_c}{b}\right). \tag{16}$$

Here the strand length, b, and number of turns, n, are constants which can be calculated from the input parameters L_{max} and D_{max} and the calculated value for γ_{min} (Eq. 11) as

$$b = \frac{L_{max}}{\cos\gamma_{min}} \tag{17}$$

$$n = \frac{b}{\pi D_o} = \frac{b\sin 54.7^\circ}{\pi D_{max}} \tag{18}$$

Therefore, for a given combination of wire diameter, D_s, and strand number, N, the braiding machine can be configured using the appropriate pick per unit length setting calculated from Eq. 14.

4 TESTING OF AMA LOAD CAPACITY

An evaluation of the accuracy of the predicted beam load capacity as a function of AMA extension and pressure, as formulated in Section 2, was carried out. It was not possible to produce a muscle actuator at a scale appropriate for this application as an inner bladder material with the correct diameter was not found to be available. Thus a larger version of the muscle actuator, with an 8.8 mm maximum outer diameter, was produced (Fig. 12) using latex surgical tubing (OD 3.2 mm, ID 1.6 mm) as the internal bladder and nylon expandable mesh (OD 4.4 mm, ID 3.2 mm) and the outer sleeve. The actuator from Fig. 12 was connected to a rigid support at one end and to a calibrated spring scale (OHAUS, 4 kg capacity) on the other end (Fig. 13). The internal bladder was inflated using an instrumented syringe (BARD Caliber Inflation Device) which provided a measure of the inflation pressure.

The procedure was performed under two static pressure conditions, 689 kPa and 413 kPa. The pressure within the bladder was increased to the static set point and held constant while the load on the actuator was increased. For each data point, the contraction force exerted by the actuator on the spring scale was

Figure 12. Photograph of a prototype artificial muscle actuator.

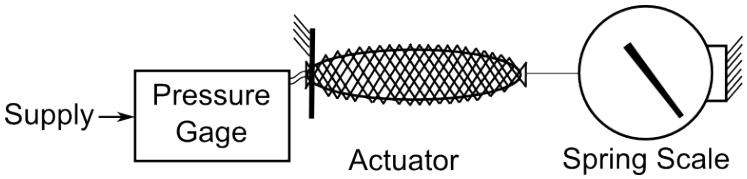

Figure 13. Illustration of test setup for measuring actuator load as a function of braid angle.

measured as well as the length of the actuator and corresponding braid angle. These results are shown in Fig. 14 where the solid line represents the predicted contraction force calculated using Eq. 8 and the dots represent the experimental data. The results show reasonable agreement, R^2 values of 0.9578 for the 689 kPa case and 0.9079 for the 413 kPa case, between the predicted and experimental forces. Better agreement was seen for the high-force, elongated actuator condition and greater discrepancy for the low-force, contracted muscle condition with the largest error occurring at a braid angle of 50° where the error is 50% of the predicted value (689 kPa case). These finding are similar to results reported in the literature Chou and Hannaford (1996); Davis and Caldwell (2006). Deviations between the experimental and theoretical actuator forces are likely due to frictional effects which become more observable at higher braid angles.

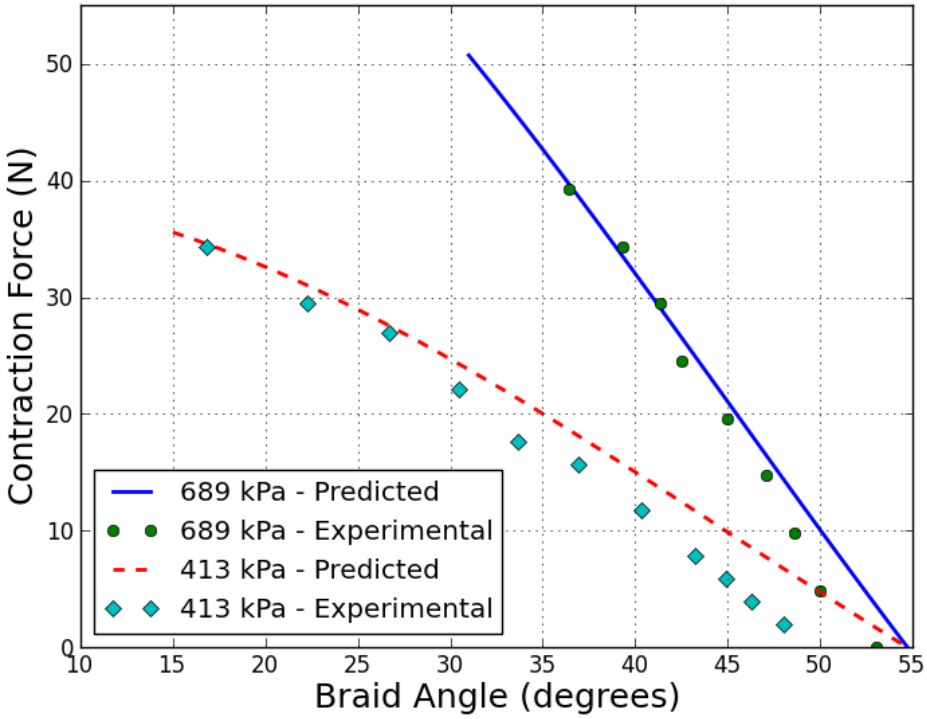

Figure 14. Plot of force output from the artificial muscle actuator predicted analytically (solid line) and determined experimentally (dots).

5 DISCUSSION

The use of artificial muscle actuators for robotic applications has been expanding as they provide several advantages including dexterous mobility and compliance when coming into contact with other surfaces or objects Trivedi et al. (2008b). This is particularly important in the application of minimally invasive surgery where the robot maneuvers in a unpredictable and sensitive environment. Further, the use of a hydraulic artificial muscle actuator for this purpose provides the opportunity for greater force output for the given size constraints, as shown in Fig. 3 where it is seen that the theoretical load capacity of the AMA is twice that of a conventional hydraulic actuator for the same diameter. In Section 2, a method for modeling the AMA and its load capacity was given showing that actuator force is a function of internal pressure and actuator length. The procedure for defining this method includes several simplifying assumptions; however, it was demonstrated that at the prototype scale for this application, the predicted output compared well with the experimental results. As was shown, the maximum contraction of the AMA is set by the braid geometry at a braid angle of $54.7°$. However, the maximum elongation of the AMA is something that can be designed and thus allows for an optimization of the AMA characteristics in order to achieve the greatest stroke length while avoiding failure.

The methods presented here make it possible to identify the appropriate braid characteristics to achieve maximum AMA performance. Maximum performance is obtained by minimizing the achievable braid angle. The minimum braid angle is dependent on the number of strands within the braided mesh and the diameter of those strands Davis and Caldwell (2006). The limiting conditions placed on these two quantities are the yield stress of the strands and the stress limit of the inner bladder. The yield stress of the strand can be calculated directly knowing the strand number, strand diameter, pressure, and braid angle of the AMA (see Eq. 12). The stress within the bladder requires more careful consideration as it is also

parameter dependent but it less well defined in terms of a solution method. Therefore, to determine bladder stress, a finite element analysis was used. Here it was shown that under all tested conditions the maximum bladder stress occurred at a braid angle of $45°$. Thus in performing an optimization calculation, the braid angle can be set at this value to eliminate one of the variables. Further, since it is desired to minimize the achievable braid angle, the bladder wall thickness can be set at a low value for this calculation as well while retaining the option of increases the thickness to permit higher operating pressures. Finally, under the appropriate stress constraints, it was shown that it is possible to calculate the smallest allowable strand diameter of the smallest number of strands that can be used to produce an usable AMA.

Using a prototype AMA, it was demonstrated that a load capacity of 40 N was possible with a bladder pressure of 689 kPa. However, this value does not represent the maximum achievable value since the muscle was not in its fully extended condition when the limit of the spring scale was reached. The theoretical prediction was found to be accurate at small braid angles. If the theoretical calculation for AMA load capacity is extended towards smaller braid angles, then the load capacity of the prototype AMA would approach 80 N as the braid angle approached $10°$. If we then extend this model to the design scale for the example application Berg (2013c), the predicted load capacity of the AMA would be 25.9 N as the braid angle approached $10°$ for the same supply pressure.

CONFLICT OF INTEREST STATEMENT

The authors declare that the research was conducted in the absence of any commercial or financial relationships that could be construed as a potential conflict of interest.

AUTHOR CONTRIBUTIONS

The Author Contributions section is mandatory for all articles, including articles by sole authors. If an appropriate statement is not provided on submission, a standard one will be inserted during the production process. The Author Contributions statement must describe the contributions of individual authors referred to by their initials and, in doing so, all authors agree to be accountable for the content of the work.

FUNDING

Partial financial support was provided by the University of Minnesota Institute for Engineering in Medicine

ACKNOWLEDGMENTS

The authors would like to thank

DATA AVAILABILITY STATEMENT

The datasets [GENERATED/ANALYZED] for this study can be found in the [NAME OF REPOSITORY] [LINK].

REFERENCES

[Dataset] Berg, D. (2013a). Abaqus script for diamond shaped pressurized plate

[Dataset] Berg, D. (2013b). FEA results for a diamond shaped pressurized plate of variable dimensions

Berg, D., Kinney, T., Li, P., and Erdman, A. (2011). Determination of surgical robot tool force requirements through tissue manipulation and suture force measurement. In *Proceedings of the 2011 Design of Medical Devices Conference* (Minneapolis, MN: ASME). DMD2011-5257

Berg, D. R. (2013c). *Design of a Hydraulic Dexterous Manipulator for Minimally Invasive Surgery*. Phd, University of Minnesota, Minneapolis, MN

Cardona, D. (2012). *A MRI Compatible Concentric Tube Continuum Robot With Pneumatic Actuation*. Master's thesis, Vanderbilt University

Chou, C.-P. and Hannaford, B. (1996). Measurement and modeling of McKibben pneumatic artificial muscles. *IEEE Transactions on Robotics and Automation* 12, 90–102. doi:10.1109/70.481753

Davis, S. and Caldwell, D. (2006). Braid effects on contractile range and friction modeling in pneumatic muscle actuators. *The International Journal of Robotics Research* 25, 359–369. doi:10.1177/0278364906063227

Davis, S., Tsagarakis, N., Canderle, J., and Caldwell, D. (2003). Enhanced modelling and performance in braided pneumatic muscle actuators. *The International Journal of Robotics Research* 22, 213–227. doi:10.1177/0278364903022003006

Granosik, G. and Borenstein, J. (2006). Pneumatic actuators for serpentine robot. In *Climbing and Walking Robots* (Springer Berlin Heidelberg). 719–726

Hagan, E., Charalambides, M., Young, C., Learner, T., and Hackney, S. (2009). Tensile properties of latex paint films with tio2 pigment. *Mechanics of Time-Dependent Materials* 13, 149–161

Klute, G. and Hannaford, B. (2000). Accounting for elastic energy storage in mckibben artificial muscle actuators. *Journal of Dynamic Systems, Measurement, and Control* 122, 386–388

Omeroglu, S. (2006). The effect of braiding parameters on the mechanical properties of braided ropes. *Fibres and Textiles in Eastern Europe* 14, 53

Schulte, H. (1961). The characteristics of the McKibben artificial muscle. In *The Application of External Power in Prosthetics and Orthotics* (National Academy of Sciences – National Research Council). 94–115

Tondu, B., Boitier, V., and Lopez, P. (1996). Théorie d'un muscle artificiel pneumatique et application à la modélisation du muscle artificiel de McKibben. *Comptes rendus de l'Académie des Sciences* 320, 105–114

Trivedi, D., Lotfi, A., and Rahn, C. (2008a). Geometrically exact models for soft robotic manipulators. *IEEE Transactions on Robotics* 24, 773–780

Trivedi, D., Rahn, C., Kier, W., and Walker, I. (2008b). Soft robotics: Biological inspiration, state of the art, and future research. *Applied Bionics and Biomechanics* 5, 99–117

Tsagarakis, N. and Caldwell, D. (2000). Improved modelling and assessment of pneumatic muscle actuators. In *Proceedings of the 2000 IEEE International Conference on Robotics and Automation*. vol. 4, 3641–3646. doi:10.1109/ROBOT.2000.845299